The time scale in concrete fracture: A model based on partitions of unity

G.P.A.G. van Zijl
Faculty of Architecture, Delft University of Technology, The Netherlands/
Civil Engineering Department, University of Stellenbosch, South Africa

G. N. Wells
Koiter Institute Delft, Delft University of Technology, The Netherlands

ABSTRACT: Intense research efforts have been put in the formulation of theories for crack initiation and propagation in concrete. Yet, little attention has been paid to the time-dependence of fracture, despite evidence of its significance. This paper reports a finite element model which captures the time scale in concrete fracture. Visco-elasticity is employed to capture bulk creep. In the fracture process zone a different time scale acts. Therefore, a rate-dependent cracking resistance is modelled. A recently developed finite element method for modelling cohesive cracks is employed. It is based on partitions of unity, by which means displacement jumps are introduced independently of the mesh structure. This avoids the requirement of dense meshes by regularised continuum approaches to model localisation, and a priori knowledge of where cracks occur for standard discrete cracking approaches via interfaces.

1 INTRODUCTION

The behaviour of concrete is highly time- and rate-dependent. The significant increase in structural resistance upon loading rate increase in the dynamic range is well-documented. However, more recently experimental evidence of rate dependence in the quasi-static range, i.e. where inertia and wave effects are negligible, has been produced by, for example Bažant and Gettu (1992), Zhou (1992) and Bažant and Xiang (1997). The time-dependent crack growth can cause delayed structural collapse, rendering the incorporation of the time scale in computational models imperative.

The mechanisms of the time dependence are not yet fully understood. The micro-structural processes in concrete, which hold the key to the rate effects, are governed by an intricate hygro-thermal-mechanical inter-dependence. This has inspired coupled approaches to model concrete behaviour (Biot 1955; Coussy 1955; Lewis and Schrefler 1998). Such an approach is computationally costly, even if a macroscopic approach is followed. This is worsened by the requirement of dense finite element meshes in localisation zones (Askes et al. 1998; de Borst et al. 2001). The alternative cohesive zone concept for modelling cracking in concrete, as traditionally applied in terms of interface elements by (Rots 1988;

Schellekens and De Borst 1993), suffers from the requirement of a priori knowledge of crack paths. A promising solution lies in a discontinuous model based on the partitions of unity concept (Wells and Sluys 2001). Such an approach is followed in this paper.

In a step towards formulating a fully coupled hygro-thermo-mechanical model for concrete fracture, which employs a discontinuous model formulation, the mechanical part is formulated in this paper. To capture the time dependence, a phenomenological approach is followed, by modelling bulk creep with linear visco-elasticity, while the finite cracking rate is captured with a rate-dependent cohesive behaviour in the discontinuity. To verify the model, the creep failure experiments by Zhou (1992) are analysed.

2 PARTITIONS OF UNITY BASED CRACK MODELLING

The displacement field in a body crossed by a discontinuity, figure 1, can be expressed as (Wells and Sluys 2001)

$$\mathbf{u} = \hat{\mathbf{u}} + \mathscr{H}_{\Gamma_d} \tilde{\mathbf{u}} \qquad (1)$$

where $\hat{\mathbf{u}}$ and $\tilde{\mathbf{u}}$ are continuous functions on Ω, $\mathscr{H}_{\Gamma_d}$ is the Heaviside jump centered at the discontinuity sur-
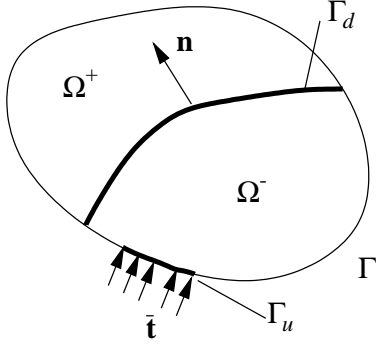
Figure 1: Body Ω crossed by a displacement discontinuity Γ_d.

face Γ_d. For finite element implementation, equation (1) is discretised to read

$$\mathbf{u} = \mathbf{N}\mathbf{a} + \mathscr{H}_{\Gamma_d}\mathbf{N}\mathbf{b} \qquad (2)$$

where $\mathbf{N}$ is a matrix containing the usual element shape functions, $\mathbf{a}$ are the regular nodal degrees of freedom and $\mathbf{b}$ are 'enhanced' nodal degrees of freedom. The displacement jump at a discontinuity is given by $\mathbf{N}\mathbf{b}$, $\mathbf{x} \in \Gamma_d$. Formally, the interpolation can be interpreted as an interpolation based on the partition of unity concept (Babuška and Melenk 1997; Duarte and Oden 1996; Wells and Sluys 2001).

The infinitesimal strain field is obtained by taking the symmetric gradient of the displacement field:

$$\nabla^{\mathrm{s}}\hat{\mathbf{u}} = \mathbf{B}\mathbf{a}, \nabla^{\mathrm{s}}\tilde{\mathbf{u}} = \mathbf{B}\mathbf{b} \qquad (3)$$

where $\mathbf{B}$ is the usual matrix containing spatial derivatives of the element shape functions. The superscript $^{\mathrm{s}}$ indicates that only the symmetric part of the displacement field gradient is taken. For convenience, the superscript will be left out of the subsequent elaborations.

The starting point for the finite element formulation is the virtual work equation, which reads without body forces:

$$\int_\Omega \nabla\boldsymbol{\eta}:\boldsymbol{\sigma}\,d\Omega = \int_{\Gamma_u} \boldsymbol{\eta}\cdot\bar{\mathbf{t}}\,d\Gamma \qquad (4)$$

where $\boldsymbol{\eta}$ are admissible displacement variations, decomposed as

$$\boldsymbol{\eta} = \hat{\boldsymbol{\eta}} + \mathscr{H}_{\Gamma_d}\tilde{\boldsymbol{\eta}}, \qquad (5)$$

$\boldsymbol{\sigma}$ is the stress field and $\bar{\mathbf{t}}$ are external traction forces (see figure 1). The gradient of admissible displacement variations is given by

$$\nabla\boldsymbol{\eta} = \nabla\hat{\boldsymbol{\eta}} + \mathscr{H}_{\Gamma_d}\nabla\tilde{\boldsymbol{\eta}} + \delta_{\Gamma_d}(\tilde{\boldsymbol{\eta}}\otimes\mathbf{n}), \qquad (6)$$

with δ_{Γ_d} the Dirac-delta function, centered at the discontinuity and $\mathbf{n}$ is the normal vector to the discontinuity, pointing to Ω^+.

Inserting equations (5) and (6) into the virtual work equation (4) leads to:

$$\int_\Omega \nabla\hat{\boldsymbol{\eta}}:\boldsymbol{\sigma}\,d\Omega + \int_{\Omega^+} \nabla\tilde{\boldsymbol{\eta}}:\boldsymbol{\sigma}\,d\Omega$$

$$+ \int_{\Gamma_d} \tilde{\boldsymbol{\eta}}_{\Gamma_d}\cdot\mathbf{t}\,d\Gamma = \int_{\Gamma_u}\left(\hat{\boldsymbol{\eta}} + \mathscr{H}_{\Gamma_d}\tilde{\boldsymbol{\eta}}\right)\cdot\bar{\mathbf{t}}\,d\Gamma \quad (7)$$

where $\mathbf{t}\,(=\boldsymbol{\sigma}\mathbf{n})$ are the traction forces acting at the surface Γ_d. The Dirac-delta term has been eliminated using the well-known integration property of the distribution.

Since equation (7) must hold for all $\hat{\boldsymbol{\eta}}$ ($\tilde{\boldsymbol{\eta}} = \mathbf{0}$), as well as for all $\tilde{\boldsymbol{\eta}}$ ($\hat{\boldsymbol{\eta}} = \mathbf{0}$), inserting the discretised expressions from equations (2) and (3) into equation (7) leads to two discrete weak governing equations (Wells and Sluys 2001):

$$\int_\Omega \mathbf{B}^{\mathrm{T}}\boldsymbol{\sigma}\,d\Omega = \int_{\Gamma_u} \mathbf{N}^{\mathrm{T}}\bar{\mathbf{t}}\,d\Gamma \qquad (8\mathrm{a})$$

$$\int_{\Omega^+} \mathbf{B}^{\mathrm{T}}\boldsymbol{\sigma}\,d\Omega + \int_{\Gamma_d} \mathbf{N}^{\mathrm{T}}\mathbf{t}\,d\Gamma = \int_{\Gamma_u} \mathscr{H}_{\Gamma_d}\mathbf{N}^{\mathrm{T}}\bar{\mathbf{t}}\,d\Gamma. \quad (8\mathrm{b})$$

The stress rate in a visco-elastic continuum can be expressed as (van Zijl et al. 2001)

$$\dot{\boldsymbol{\sigma}} = \mathbf{D}^{ve}\left(\mathbf{B}\dot{\mathbf{a}} + \mathscr{H}_{\Gamma_d}\mathbf{B}\dot{\mathbf{b}}\right) + \boldsymbol{\Sigma} \qquad (9)$$

where $\mathbf{D}^{ve}$ is an equivalent, time-dependent stiffness modulus and $\boldsymbol{\Sigma}$ is a viscous stress term which accounts for the history. The traction rate at a discontinuity can be expressed as

$$\dot{\mathbf{t}} = \mathbf{T}\mathbf{N}\dot{\mathbf{b}} \qquad (10)$$

where $\mathbf{T}$ relates the instantaneous traction and displacement jump rates. Inserting the stress and traction rate expressions into equation (8) and employing a linear time integration scheme gives

$$\mathbf{K}\begin{Bmatrix}\Delta\mathbf{a}\\\Delta\mathbf{b}\end{Bmatrix} = \begin{Bmatrix}\mathbf{f}_{\mathrm{e,a}}\\\mathbf{f}_{\mathrm{e,b}}\end{Bmatrix} - \begin{Bmatrix}\mathbf{f}_{\mathrm{i,a}}\\\mathbf{f}_{\mathrm{i,b}}\end{Bmatrix} \qquad (11)$$

where the stiffness matrix $\mathbf{K}$ has the form:

$$\begin{bmatrix} \int_\Omega \mathbf{B}^{\mathrm{T}}\mathbf{D}^{ve}\mathbf{B}\,d\Omega & \int_{\Omega^+}\mathbf{B}^{\mathrm{T}}\mathbf{D}^{ve}\mathbf{B}\,d\Omega \\ \int_{\Omega^+}\mathbf{B}^{\mathrm{T}}\mathbf{D}^{ve}\mathbf{B}\,d\Omega & \int_{\Omega^+}\mathbf{B}^{\mathrm{T}}\mathbf{D}^{ve}\mathbf{B}\,d\Omega + \int_{\Gamma_d}\mathbf{N}^{\mathrm{T}}\mathbf{T}\mathbf{N}\,d\Gamma \end{bmatrix}$$
$$(12)$$

Note that a semi-analytical time integration is performed (van Zijl et al. 2001b) for an accurate solution of the history. Thereby, the history term is assumed to

be constant during a time increment and does not appear in the stiffness matrix. The internal and external force vectors are equal to:

$$\mathbf{f}_{e,a} = \int_{\Gamma_u} \mathbf{N}^T \bar{\mathbf{t}} \, d\Gamma \tag{13a}$$

$$\mathbf{f}_{e,b} = \int_{\Gamma_u} \mathscr{H}_{\Gamma_d} \mathbf{N}^T \bar{\mathbf{t}} \, d\Gamma \tag{13b}$$

$$\mathbf{f}_{i,a} = \int_{\Omega} \mathbf{B}^T \boldsymbol{\sigma} \, d\Omega \tag{13c}$$

$$\mathbf{f}_{i,b} = \int_{\Omega^+} \mathbf{B}^T \boldsymbol{\sigma} \, d\Omega + \int_{\Gamma_d} \mathbf{N}^T \mathbf{t} \, d\Gamma. \tag{13d}$$

See Wells and Sluys (2001) for a detailed discussion of implementation aspects.

3 CONSTITUTIVE MODEL

The stress rate equation (9) can be integrated with a linear scheme, which produces the stress increment during the time increment Δt

$$\Delta\boldsymbol{\sigma} = \mathbf{D}^{ve}\left(\mathbf{B}\Delta\mathbf{a} + \mathscr{H}_{\Gamma_d}\mathbf{B}\Delta\mathbf{b}\right) + {}^t\tilde{\boldsymbol{\sigma}}, \tag{14}$$

where

$$\mathbf{D}^{ve} = \left[E_0(t^*) + \sum_{n=1}^{N}\left(1 - e^{-\frac{\Delta t}{\zeta_n}}\right)\frac{E_n(t^*)}{\Delta t/\zeta_n}\right]\mathbf{D}$$

$${}^t\tilde{\boldsymbol{\sigma}} = -\sum_{n=1}^{N}\left(1 - e^{-\frac{\Delta t}{\zeta_n}}\right){}^t\boldsymbol{\sigma}_n. \tag{15}$$

In this model an aging Maxwell chain can be identified, with time dependent element stiffnesses $E_n(t)$ and viscosities $\eta_n = E_n\zeta_n$, ζ_n being the relaxation time of chain element $n=1,2,...,N$. The stress vector ${}^t\boldsymbol{\sigma}_n$ contains the stress components in chain element n at the end of the previous time step, i.e. at time t. Note that the parameters are assumed to be constant in each time interval and are evaluated at a time $t \le t^* \le t + \Delta t$. $\mathbf{D}$ is the matrix representation of the fourth order tensor

$$D_{ijkl} = \frac{1}{1+\nu}\left[\frac{\nu}{1-2\nu}\delta_{ij}\delta_{jk} + \frac{1}{2}\left(\delta_{ik}\delta_{jl} + \delta_{il}\delta_{jk}\right)\right] \tag{16}$$

which is dependent on Poisson's ratio ν.

A discontinuity is extended when the maximum principal stress at any integration point in the element ahead of the discontinuity tip exceeds the tensile strength f_t. A rate-dependent cracking normal traction (Wu and Bažant 1993; van Zijl et al. 2001) of the form

$$t_n = f_t \exp\left(-\frac{f_t}{G_f}\kappa\right)\left[1 + k_0 \sinh^{-1}\left(\frac{\dot{\kappa}}{\dot{\kappa}_r}\right)\right]$$
$$+ k_0\,k_1\,f_t \sinh^{-1}\left(\frac{\dot{\kappa}}{\dot{\kappa}_r}\right) \tag{17}$$

is assumed in the discontinuity, where κ is the historically largest crack normal opening displacement, G_f is the fracture energy and $\dot{\kappa}_r$ is a constant, reference crack opening velocity, which, together with the model parameters k_0 and k_1 are obtained by inverse analysis of experiments at various (quasi-static) loading rates.

The shearing traction t_s is given by:

$$t_s = k_s\tilde{u}_s \tag{18}$$

where k_s is independent of the normal opening to preserve symmetry of the global stiffness matrix.

For unloading, the secant stiffness is used. The loading and unloading behaviour of a body containing the described discontinuity is illustrated in figure 2.
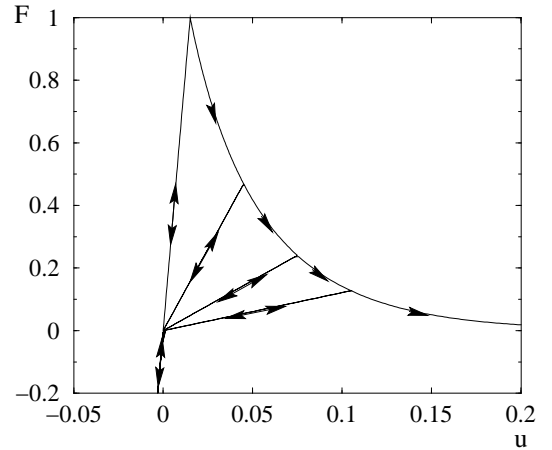

Figure 2: Uniaxial loading and unloading behaviour.

4 CASE STUDY

To study the time scale in concrete fracture, the case of failure under sustained load is investigated. The three-point bending experiments by Zhou (1992) are analysed. The specimens were 800mm long concrete beams with section 100mm × 100mm and a central notch 4mm wide and 50mm deep. The specimens were sealed to avoid drying. The results of
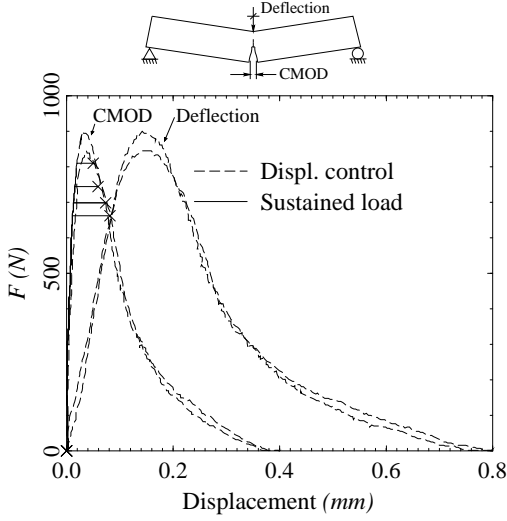
Figure 3: Three-point bending test experimental results (Zhou 1992).

two displacement-controlled experiments at a constant, central deflection rate of 5 μm.s^{-1}, as well as creep experiments at sustained loads of 92%, 85%, 80% and 76% of the peak load are shown in figure 3.

The experiments were analysed recently with a rate-dependent continuum plasticity model by van Zijl et al. (2001). They are re-analysed to verify the current model, before turning to cases where the superiority of the partition of unity based model is exploited.

The material parameters were obtained by van Zijl et al. (2001) from separate experiments by Zhou (1992): Young's modulus 30 kN.mm^{-2}, tensile strength f_t=2.66 N.mm^{-2} and fracture energy G_f=0.035 N.mm^{-1}. For this particular case the response is insensitive to the shear stiffness coefficient k_s. A 10-element Maxwell chain was fitted to relaxation test data (figure 4).
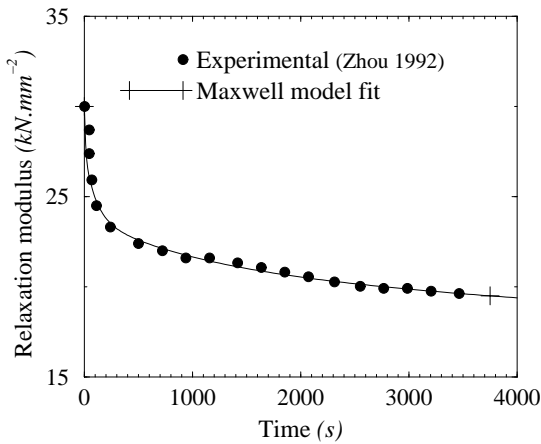

Figure 4: Relaxation modulus employed.

Furthermore, Zhou performed three-point bending tests at various loading rates on notched beams, from which the cracking rate model parameters could be
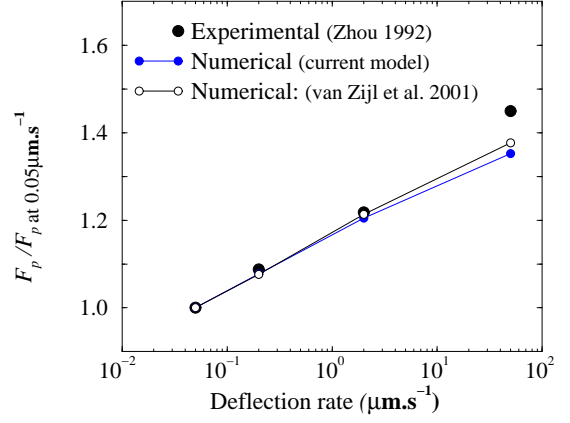

Figure 5: Loading rate effect on peak strength.

obtained by inverse analysis. The parameters obtained in this way are $k_0 = 0.05, k_1 = 0.01, \dot{\kappa}_r = 4 \times 10^{-7}$ mm.s^{-1}. The rate dependence of the peak strength is shown in figure 5. The first two parameters are the same as employed by van Zijl et al. (2001), while the reference cracking rate is obtained from the reference *strain* rate by multiplication with the crack band width l_b=4 mm. A weaker rate enhancement can be seen in figure 5 for the current model. This is due to the different constitutive model employed here. No attempt has been made to improve the paramaters to obtain a better agreement with the experimental results.

Firstly, the displacement-controlled case (central deflection rate 5 μm.s^{-1}) is analysed. Good agreement is obtained with the experimental results, as well as with the continuum model results (figure 6).
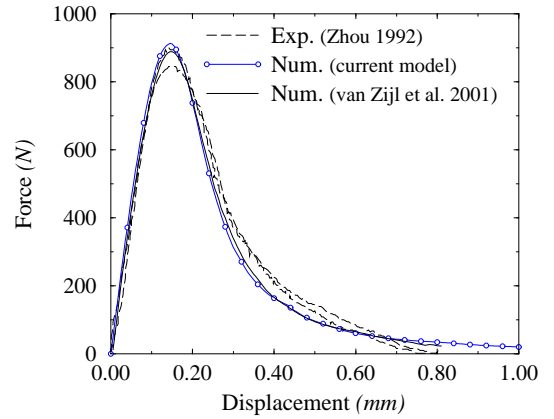

Figure 6: Three-point bending results at fixed loading rate.

To study the mesh dependence, a coarse mesh and a refined mesh are employed for the analysis. In figure 7 it can be seen that the response is insensitive to the mesh. In the subsequent analyses, the coarse mesh is employed.

Next, the creep experiments are analysed. The numerical responses are shown in figure 8. The experimental observation (figure 3) that the constant velocity response forms an envelope for creep failure is
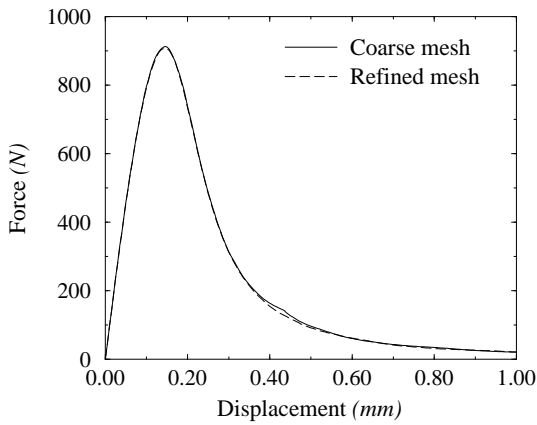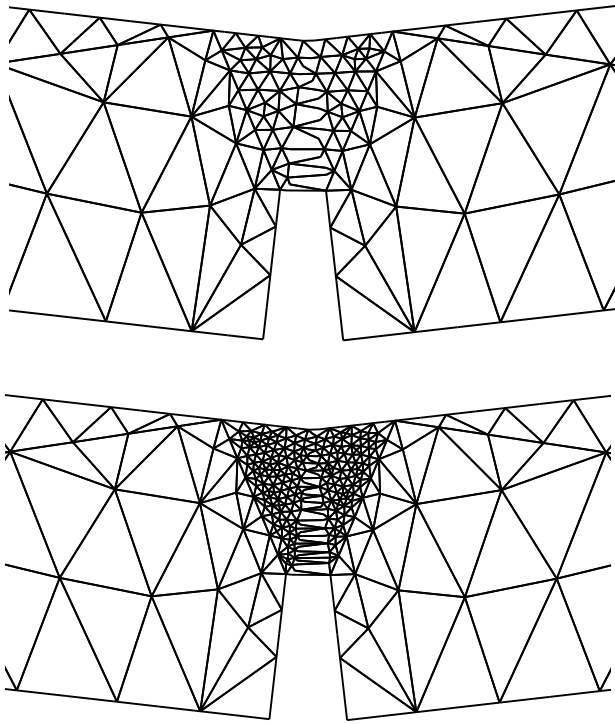
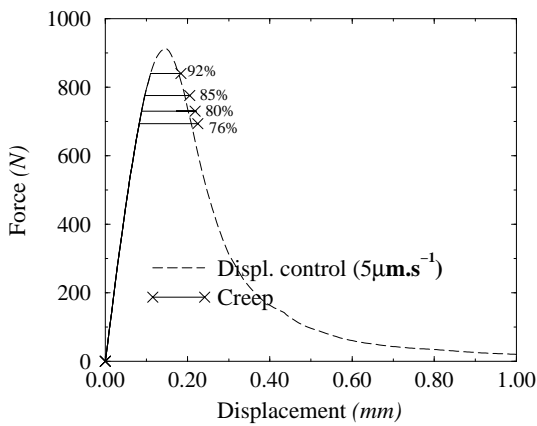Figure 7: Load-displacement response for three-point bending analysis.

Figure 8: Numerical prediction of failure under sustained load.

confirmed by the numerical results. In the creep analyses by van Zijl et al. (2001), displacement control was resumed once the point of failure under the sustained load was approached, to ensure that failure, or the inability of the beams to resist the sustained central load, was indeed imminent. In the current study a negative diagonal term in the stiffness matrix is assumed to indicate failure under the sustained load.

It is most important that the time scale of fracture is captured accurately. In figure 9 the times between the instant the full sustained load is applied and failure are shown. Good agreement is found with the experiments. The discrepancy with the numerical results by van Zijl et al. (2001) is ascribed to the different constitutive model, which also led to the lower peak load enhancement with loading rate, seen in figure 5. Also shown in figure 9 are the times to failure if the finite cracking rate is not considered, in which case the times to failure are overestimated by several orders of magnitude.
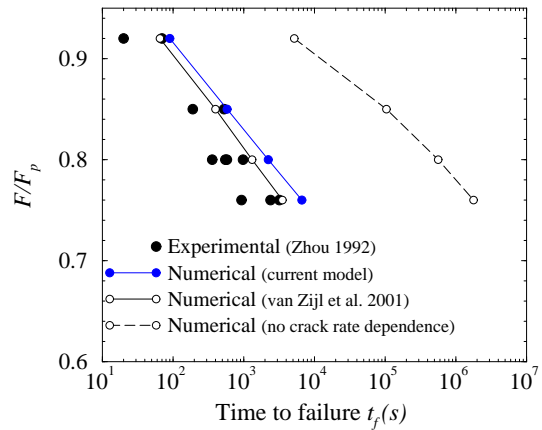

Figure 9: Time to failure under sustained load.

5 CONCLUSIONS

The extension of a cohesive zone model to incorporate the time scale in concrete fracture, has been presented. The model is based on partitions of unity. Displacement discontinuities can traverse arbitrarily through a finite element mesh avoiding a priori crack path knowledge required by discontinuity modelling via interfaces. Also, there is no requirement for dense meshes in fracture process zones, as in the case of regularised continuum approaches to crack modelling.

To capture the time scale of concrete fracture, a phenomenological approach has been followed. Two sources of time dependence have been included in the mechanical constitutive behaviour, namely linear visco-elasticity in the continuum to capture bulk creep, and a rate-dependent normal traction in the displacement discontinuity, to simulate the finite crack rate. This simplified approach has been shown to introduce the time scale accurately, through the analyses of creep failure experiments.

REFERENCES

Askes, H., Bodé, L. and Sluys, L.J. (1998). ALE analyses of localisation in wave propagation problems. *Mechanics of Cohesive-Frictional Materials 3*, 105–126.

Babuška, I. and J. M. Melenk (1997). The Partition of Unity Method. *International Journal for Numerical Methods in Engineering 40*(4), 727–758.

Bažant, Z.P. and Gettu, R. (1992). Rate effects and load relaxation in static fracture of concrete. *ACI Materials Journal 89*(5), 1–20.

Bažant, Z.P. and Xiang, Y. (1997). Crack growth and lifetime of concrete under long term loading. *Journal of Engineering Mechanics 123*(4), 350–358.

Biot, M.A. (1955). Theory of elasticity and consolidation for a porous anisotropic solid. *Journal of Applied Physics 26*(2), 182–185.

Coussy, O. (1955). *Mechanics of porous media*. John Wiley & Sons, Chichester.

de Borst, R., Wells, G.N. and Sluys, L.J. (2001). Some observations on embedded discontinuity models. *Enigneering Computations* (submitted).

Duarte, C. A. and J. T. Oden (1996). H-p clouds – an h-p meshless method. *Numerical Methods for Partial Differential Equations 12*(6), 673–705.

Hillerborg, A., M. Modeer, and P. E. Petersson (1976). Analysis of crack formation and crack growth in concrete by means of fracture mechanics and finite elements. *Cement and Concrete Research 6*(6), 773–782.

Lewis, R.W., Schrefler, B.A. (1998). *The finite element method in static and dynamic deformation and consolidation of porous media*. John Wiley & Sons, Chichester.

Rots, J.G. (1988). *Computational modelling of concrete fracture*. Ph. D. thesis, Delft University of Technology.

Schellekens, J. C. J. and R. De Borst (1993). On the numerical integration of interface elements. *International Journal for Numerical Methods in Engineering 26*(1), 43–66.

van Zijl, G.P.A.G., de Borst, R. and Rots, J.G. (2001). The role of crack rate dependence in the long-term behaviour of cementitious materials. *International Journal of Solids and Structures*(in press).

van Zijl, G.P.A.G., de Borst, R. and Rots, J.G. (2001b). A numerical model for the time-dependent cracking of cementitious materials *International Journal for Numerical Methods in Engineering*(in press).

Wells, G. N. and L. J. Sluys (2001). A new method for modelling cohesive cracks using finite elements. *International Journal for Numerical Methods in Engineering 50*(12), 2667–2682.

Wu, Z.S. and Bažant, Z.P.(1993). Finite element modelling of rate effect in concrete fracture with influence of creep. *Creep and Shrinkage of Concrete*, E.&F.N.Spon, London, 427–432.

Zhou, F.P. (1992). *Time dependent crack growth and fracture in concrete*. Ph. D. thesis, Lund University, Sweden.